Shaping of 3YSZ Porous Substrates for Oxygen Separation Membranes

Juan A. Escribano, Julio García-Fayos, José M. Serra[*]

[1]*Instituto de Tecnología Química (UPV-CSIC), Universitat Politècnica de València, Consejo Superior de Investigaciones Científicas, Avenida de los Naranjos s/n, 46022 Valencia, Spain*

[*]jmserra@itq.upv.es

Abstract

In recent years, asymmetric membranes based on mixed ionic-electronic conductors (MIEC) have gained importance in practical gas separations. MIEC ceramic materials show high-energy efficiency and high-temperature resistance, which allows direct integration in industrial processes. Thin layers are supported on porous substrates that provide mechanical strength. In the asymmetric membrane manufacture, the control of support porosity and microstructure is crucial. Colloidal processing is an interesting method that allows controlling the final microstructure in both surfaces and bulk, with high reproducibility. Here, the development of asymmetric membranes with a top functional layer made of $Ce_{0.8}Gd_{0.2}O_{1.9}/Ni_2FeO_4$ composite is presented and aims to maximize oxygen permeation and membrane robustness. The porous substrate is prepared by slip casting while the functional layers by screen-printing. The effect of pore former volume and particle morphology were studied. The combination of spherical and flake-like PMMA particles enabled to generate open porosity suitable for fast gas transport.

1 Introduction

Oxygen production has high impact in several industries due to both its use as a reagent in chemical processes and its use to provide a more efficient combustion in thermal processes. Therefore, there is a need to efficiently produce high-purity oxygen at different scales. The main way to obtain oxygen is by cryogenic distillation of air [1]. However, this process presents important drawbacks related to the high energy requirements and large plant size. One of the alternatives is the use of gas-separation ceramics membranes, which allows the selective permeation of the oxygen by diffusion through the ceramic oxide lattice. Among other advantages, ceramic membranes allow the *in situ* O_2 production at small-to-medium scale where other technologies such as the cryogenic are not economically feasible. This kind of membranes should present both ionic and electronic conductivity [2,3], since oxygen permeates thanks to the presence of oxygen vacancies in the crystalline lattice driven by the oxygen pressure gradient across the membrane, and a counter-diffusion of electrons occurs to balance the charge at both sides of the membrane. In contrast to the difficulty to find a single materials with high thermo-chemical stability and proper mixed ionic-electronic conduction, dual-phase composite materials have enabled reaching promising results [4]. In this paper, a combination of a spinel Ni_2FeO_4 (NFO) and a fluorite $Ce_{0.8}Gd_{0.2}O_{2-\delta}$ (CGO) is used, obtaining a stable composite material able to permeate oxygen [5,6]. NFO spinel could present both n-type and p-type electronic conductivity depending on the different synthesis techniques and crystal sizes. The n-type behavior has been attributed to the presence of Fe^{2+}, which enables the electron hopping from Fe^{2+} to Fe^{3+}. The p-type behavior has been related to the presence of Ni^{3+} and hole hopping from Ni^{3+} to Ni^{2+}. The last can be assigned to the deficiency or excess in Ni, because a Ni excess corresponds to Fe^{3+} deficiency compensated with Ni^{3+} (p-type) while a Ni deficiency corresponds to a Fe^{2+} compensation (n-type)[7]. On the other hand, the CGO present high ionic conductivity and stability [8,9] and together with NFO generates a composite material with high O_2 permeation features but due to the presence of two phases, the influence of the grain boundary is relevant.

When the oxygen flux is determined by the transport through the membrane bulk, the flux at the steady state through membrane can be describe by the Wagner equation:

$$j_{O_2} = \frac{RT}{16F^2} \sigma_{amb} \frac{1}{L} ln \frac{p'_{O_2}}{p''_{O_2}} \qquad (1)$$

where R is the gas constant (J/Kmol), T is the temperature (K), F is the Faraday constant (C/mol), σ_{amb} is the ambipolar conductivity, L is the membrane thickness (m) and p'_{O2} and p''_{O2} are the oxygen partial pressure at both membrane sides. Note that, for a sufficiently thin membrane, the permeation can be limited by other phenomena such as oxygen surface gas-solid exchange, gas transport in the porous substrate and gas transport in the open gas chambers.

According to the Wagner equation (1), a membrane should be as thin as possible in order to optimize the permeation flux. In this sense, asymmetric membranes allow reaching thin layers of the separation membrane with high mechanical properties without decreasing their flux properties [10,11]. These membranes are constituted by a dense layer of MIEC material/composite deposited on a porous substrate [12]. There is a wide range of techniques that allows preparing thin layers on different substrates [13–15]. The choice of the technique must be in accordance with the characteristics of both the layer and the substrate. For asymmetric membranes, suspension-spraying and screen-printing processes allow the

deposition of the membrane layer with controller thickness with high reproducibility and superficial quality on plane substrate of different areas.

The requirements of the porous support respect to the MIEC layer are that they should present chemical compatibility, similar thermal expansion coefficient, good gas permeation and excellent mechanical properties under operation conditions [16]. In this sense, 3 mol% Yttria stabilized Zirconium (3YSZ) meets the requirements as substrate, due to it high chemical stability and high mechanical properties. As for the layer deposition, there are numerous processing routes to obtain porous 3YSZ substrate. In the recent years, substrate processing of asymmetric membranes has been focused in tape casting [17,18], freeze casting [19,20], pressing [21,22] and extrusion processing [23,24], while slip casting has been received less attention [25,26]. In previous works on membrane manufacture by slip casting, the porosity in the substrate was induced by careful control of (i) the particle size during processing and (ii) the thermal treatment. However, the use of pore-former particles enables to tailor the porosity and sinter the substrate at higher temperatures without much porosity loss, what in turn increases the membrane mechanical properties. On the other hand, slip casting is one of the most common industrial methods for ceramic processing that provides high dispersion degree of ceramic phases and accurate control of the microstructure in cast porous materials [27,28]. Slip casting is a simple, industrially and economically viable shaping technique and allows obtaining complex geometries/morphologies than other processing techniques. In addition, the colloidal processing implies the formation of suspensions in aqueous media, which is a drawback in the case of both non-oxide ceramic and metal particles, due to the elevated reactivity of these materials with the suspension media. From an electrochemical point of view, water is one of the more complex liquid media to work with. It has a very high polar moment, which requires careful control of the conditions of the suspensions [29,30].

The present work focuses on the development of asymmetric membranes by different processing methods with a top functional layer made of the $Ce_{0.8}Gd_{0.2}O_{1.9}/Ni_2FeO_4/$ (CGO-NFO) dual-phase material with the aim to maximize oxygen permeation and membrane robustness under harsh operation conditions, i.e. high temperature, important pressure gradient across the membrane and high CO_2 concentrations. In this case, the porous substrate of the membrane is prepared by slip casting while the functional layer by screen-printing.

2 Materials and methodology

The membrane substrates were prepared using a commercial 3YSZ powder (TZ-3YS-E, TOSOH Corporation, Japan) with 90 nm of average particle size, a specific surface area of 7.30 m^2/g and 6.05 g/cm^3 of density. A micrograph of the as received powders is present in Figure 1. As can be observed, the 3YSZ powder is formed by agglomerates of nanometric particles.
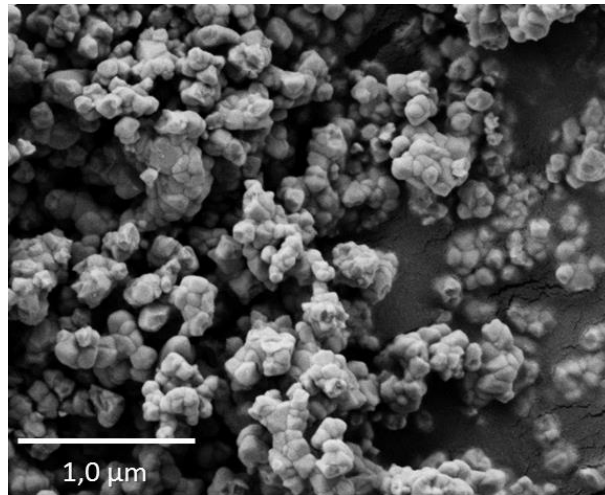
Figure 1 Micrograph of the 3YSZ powder as received

The characterization of the colloidal properties of the 3YSZ comprised the zeta potential measurement as a function of pH and was performed using a suspension with a solid content of 0.1 g/L in 10^{-2}M KCl, using HTMA and HNO_3 to adjust the pH. Measurements were carry out using a Zetasizer Nano ZS (Malvern, UK).

In order to introduce porosity in the microstructure of the final body, different polymethylmethacrylate (PMMA) powders were added to the 3YSZ slurries. Table 1 presents the characteristics of the pore formers used in the slurries, and Figure 2 shows the corresponding SEM micrographs.

Table 1 Morphological characteristics of the PMMA particles

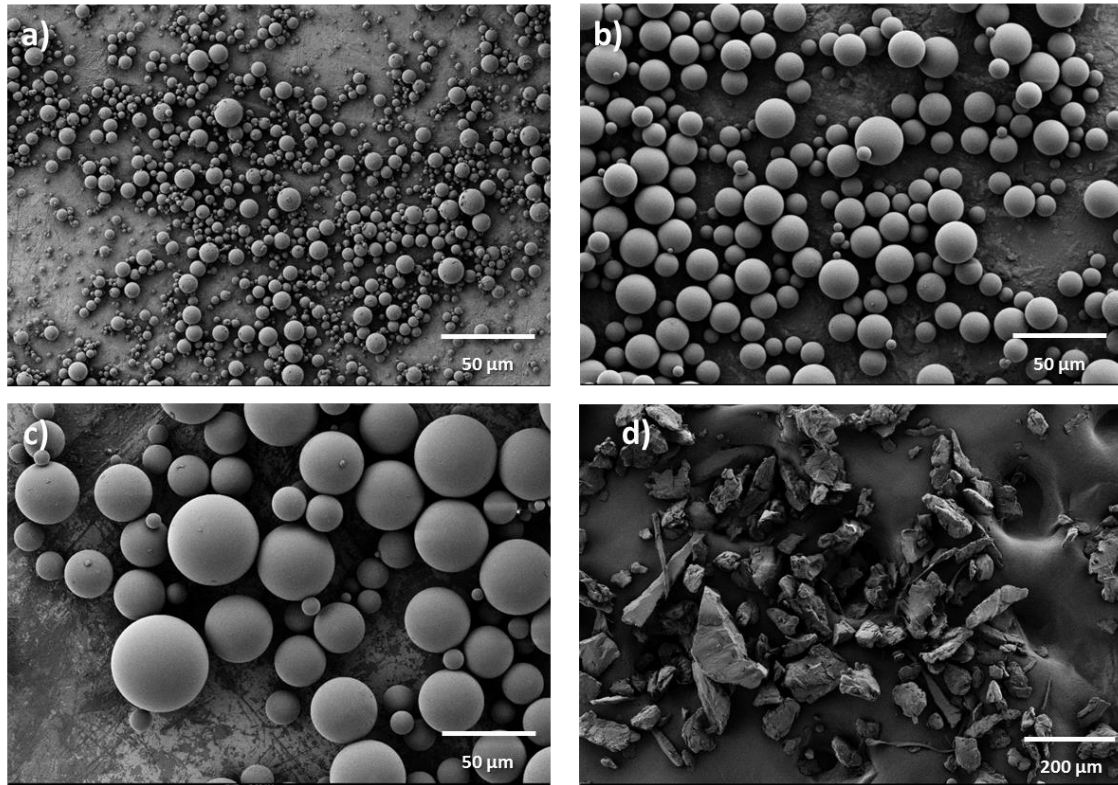| Code	Size dv50 (µm)	Morphology	Reference
S-006	6.0	Spherical	MX-500, Esprix (USA)
S-020	20	Spherical	MX-2000, Esprix (USA)
S-050	50	Spherical	Altuglass BS100, Arkema (France)
F-150	150	Flakes	Porlat K85, Zschimmer & Schwarz (Germany)

Figure 2 Micrographs of the pore former used a)S-006, b) S-020, c) S-050 and d) F-150

To measure the rheology, a Haake Mars rheometer (Thermo Scientific, Germany) with a double-cone plate fix of 60 mm of diameter and angle of 2º (DC60/2º) was used. Tests were performed in a control rate mode (CR) shearing from 0 to 1000 s^{-1} in 2 minutes, dwelling at 1000 s^{-1} for 1 minute and shearing down to 0 s^{-1} in 2 minutes and control stress from 0 to 6 Pa in 2 minutes and down to 0 Pa in the same time. All tests were done at a constant temperature of 23 ± 0.5ºC. The applied high-shear rates during up-ramps are enough to achieve a reproducible suspension microstructure, dependent only on the suspension composition, but not on the slurry preparation history [31]. The flow curves were fitted using the Cross model (eq. 2), which describes the pseudoplastic behavior.

$$\eta = \eta_\infty \frac{\eta_0 - \eta_\infty}{1 + (CY)^n} \qquad (2)$$

where η_0 and η_∞ are the extrapolation of the viscosity to zero and infinity respectively, C is a time constant and n is the rate constant, and it is a parameter which is related with the dependence of viscosity on the shear rate. The Cross model describes the limit behavior of the standing suspension and at infinite shear rate, therefore not only gives information about suspension viscosity but about its stability.

For the MIEC membrane layers, a combination of $Ce_{0.8}Gd_{0.2}O_{1.9}$ and Ni_2FeO_4 (CGO-NFO) was prepared by solid state reaction method, comprising the sintering of the ball-milled single oxides at 1250 ºC followed by further ball milling. The particle size of the powder is between 0.9 µm to 10.1 µm, with a dv_{50} of 3.0 µm. The MIEC layer was deposited onto the substrates by screen-printing, using a dispersion of the composite in terpineol with ethylcellulose as described in previous papers [14]. In order to improve the mechanical and thermal stability of the membrane and the thermal expansion compatibility, a porous interlayer was deposited

using 1.5 μm PMMA particles as pore former. The inks were refined using a three-roller mill and its rheological behavior was also studied.

The density and porosity of the substrates was determined by Archimedes method according to the ASTM C373-88 [32], using the following equation (eq. 3)

$$P = \frac{M-D}{M-S} \cdot \rho_{H_2O} \cdot 100 \qquad (3)$$

where P is the open porosity, M is the mass of the water-saturated sample, D the mass of the dry sample, S is the mass of the sample immersed in water and ρ_{H2O} is the density of the water at the experiment temperature. The microstructure of the sintered samples was registered using a XL-30 scanning electron microscope (Philips, Netherlands).

The in-plane electrical conductivity of the films was measured by standard four-point DC technique on films deposited on 3YSZ substrates by using silver wires and paste for contacting. Measurements were recorded as the temperature decreases from 800 to 400 °C at 1 °C/min at a constant atmosphere, in different oxygen partial pressures (pO_2). The constant current was supplied by a programmable current source (Keithley 2601), and the voltage drop through the sample was detected by a multimeter (Keithley 3706).

Oxygen permeation studies were carried out in a lab-scale quartz reactor. Synthetic air (21 vol. % O_2 in the feed stream) or pure oxygen was fed in to the oxygen-rich chamber, while argon was used as the sweep gas on the permeate side. Both gases were fed at atmospheric pressure. Inlet gases were preheated in order to ensure the correct gas temperature for contact with the membrane surface. This is particularly important when high gas flow rates are employed. All streams were individually mass flow controlled. The temperature was measured by a thermocouple attached to the membrane. A PID controller maintained temperature variations within 2ºC of the set point.

3. Results

3.1 Porous substrates

For the wet processing techniques as slip casting, the main requirement is to obtain a stable suspension and, for this purpose, the use of different additives as organic molecules is a common practice [29]. These additives modify the colloidal behavior of the solid particles in the suspension, improving their stability and allowing increasing the solid content of the slurries. Figure 3 plots the zeta potential of the 3YSZ as a function of pH suspension with and without an anionic dispersant. As shown in Figure 3, 3YSZ presents an isoelectric point of 5.5 and a maximum superficial charge of -16 mV at pH 10. The addition of 0.4 wt. % of Dolaplix CE64 (Zchimmer & Schwartz, Germany) causes that the isoelectric point of the 3YSZ shifts to 4.3 and the maximum repulsion value increases to -26 mV at pH 10, allowing obtaining more stable 3YSZ suspensions.
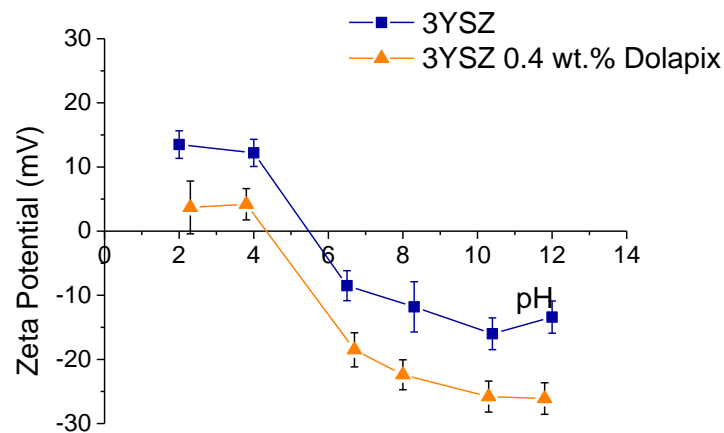
Figure 3 Zeta potential vs. pH of the 3YSZ powder and 3YSZ powder with 0.4 wt. % of Dolapix CE64.

According to the zeta potential study, the casting slurries were prepared at pH 10 in water with a 0.4 wt. % of Dolaplix. Aiming to produce porous 3YSZ substrates, pore former particles were added to the 3YSZ slurry in two different amounts, 40 vol. % and 60 vol. %. The solid content was set at 35 vol. % for all the suspensions. The effect of the addition of the pore former contents in the rheology was also studied. Figure 4 presents the flow curves of the 3YSZ slurries without pore former, with 40 vol. % of S-050 and with 60 vol. % in a logarithmic plot.
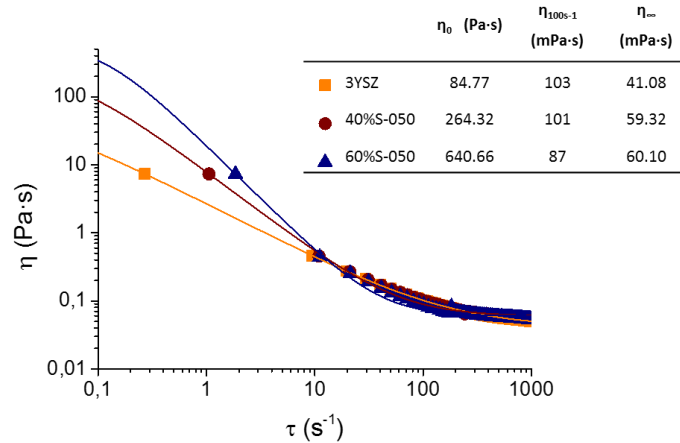
Figure 4 Logarithmic plot of the viscosity versus shear rate for the 3YSZ slurries with different amount of S-050 and them rheological parameters

All the slurries present a pseudo plastic behavior with viscosities at shear rates of 100 s^{-1} close to 100 mPa·s and therefore are suitable for slip casting. The slurries were casted in a plaster mold using a plastic cylinder, dried at room temperature and sintered at 1450ºC for 2 h. The sintered samples were characterized based on their microstructure and density. *Figure 5* shows the SEM micrographs of polished cross-sections for the substrates casted using 3YSZ slurries with 40 vol. % of S-005 (*Figure 5*a), S-020 (*Figure 5*b) and S-050 (*Figure 5*c). In order to improve the porosity and it interconnectivity, the pore former addition was increased to 60 vol. %, and also an irregularly-shaped PMMA particles (F-150) were studied. In *Figure 6*, the microstructures of the polished cross-sections for the samples processed with 60 vol. % of S-020 (*Figure 6*a), S-050 (*Figure 6*b) and F-150 (*Figure 6*c) can be observed.
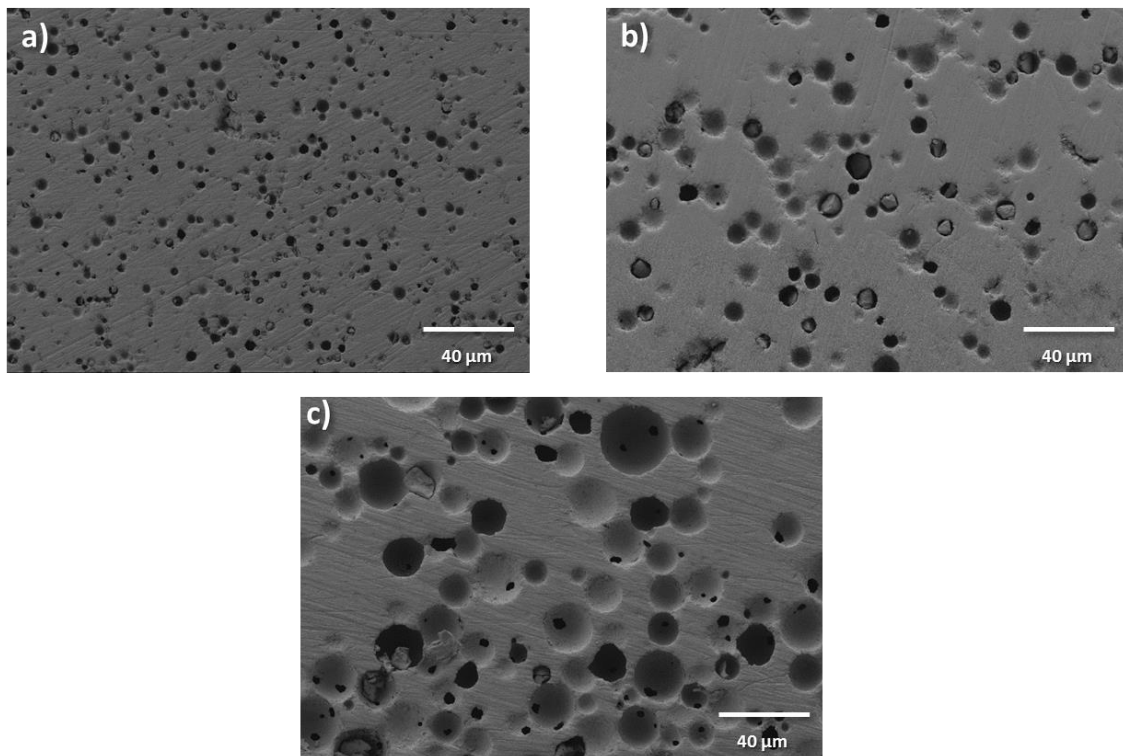

Figure 5 Microstructure of the 3YSZ samples from the suspensions with 40 vol% of a) S-005, b) S-020 and c) S-050.
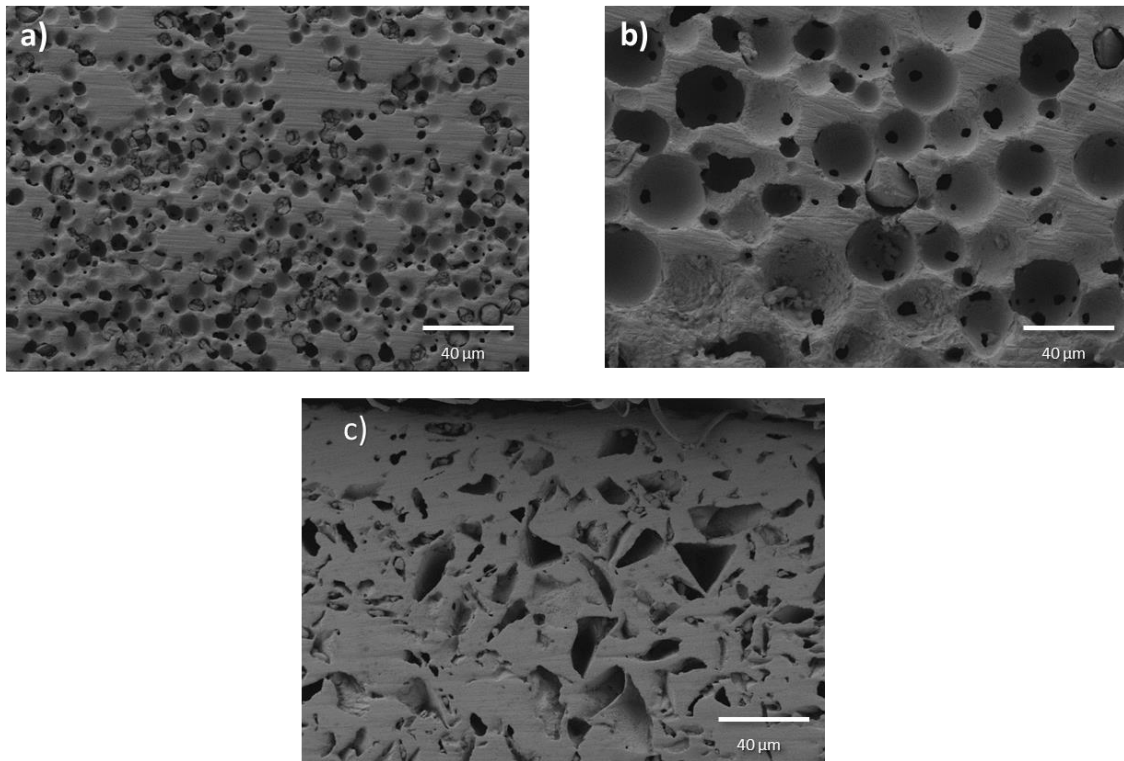
Figure 6 Microstructure of the 3YSZ samples from the suspensions with 60 vol. % of a) S-020, b) S-050 and c) F-150.

It should be noted that for both sets of samples, the formed pores present a shape and size related to the original pore former as could be expected. As a consequence, the use of spherical pore-former particles produces more closed porosity even for the samples with 60 vol. % of pore former. Due to the requirement of interconnectivity between pores to allow the gas diffusion during membrane operation, an improvement in the microstructure was done by mixing spherical-like pore former S-050 with F-150 flake shaped particles (Figure 7).
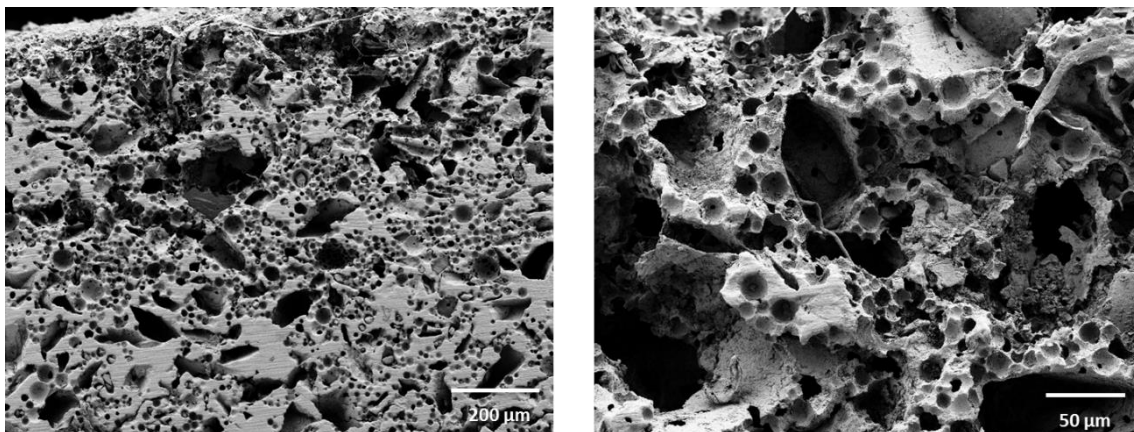

Figure 7 Micrographs of the F-150+S-050 sample

In addition to the microstructure study, the density of the sintered substrates was determined by Archimedes method. *Table 2* summarizes the values of the relative porosity of all the substrates prepared and are compared with the pore former fraction added in the slurries.

Table 2 Porosity of the prepared substrates at 1450º C comparing to the volume of pore former added in the slurry

Pore Former	PMMA vol%	Rel. Porosity (at 1450ºC)
S-006	40	23%
S-020	40	25%
S-050	40	25%
S-006	60	40%
S-020	60	44%
S-050	60	47%
F-150	60	48%
F-150+S-050	60	50%

In order to characterize the permeation properties of the substrates, the flow resistance of the samples was measured in terms of pressure drop (Δp) as a function of the imposed air flow rate at ambient pressure and room temperature (Figure 8). As SEM and porosity analyses revealed, the samples prepared from suspensions with 40 vol. % of pore former do not present enough open porosity at all and gas flow was negligible for these samples. Therefore, the pressure drop could be measured only for the samples prepared from suspensions containing a 60 vol. % of pore former.
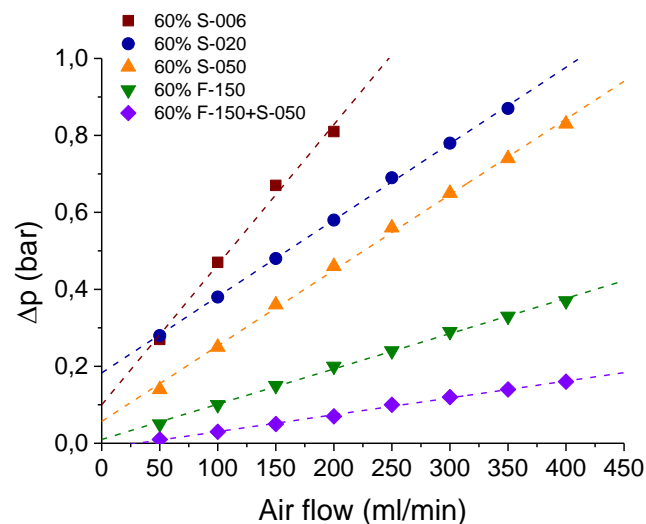

Figure 8 Pressure drop measurement as a function of the air inlet flow rate through the substrates.

As expected for the porous bodies, all the samples present increasing pressure drop with higher air flow rates. Comparing the values in the *Figure 8* it can be ascertained that the increment in PMMA particle size causes a decrease in the pressure drop, being a major difference when F-150 particles are used. For the S-050 sample, the pressure decreases 0.48 bar at 200 ml/min, while for the F-150 sample the pressure drops to 0.19 bar at the same air flow rate. As previously observed at the micrographs in *Figure 7*, the combination of F-150 and

S-050 particles improve the pore connectivity, which is reflected in the decreased pressure drop, i.e. down to 0.07 bar at 200 ml/min.

3.2 MIEC layer

The MIEC layer and the porous interlayer were deposited by screen-printing. The ink was prepared by dispersing the solid powders in a dissolution of 6 wt. % ethylcellulose in terpineol. The rheological behavior of both inks is presented in *Figure 9*.
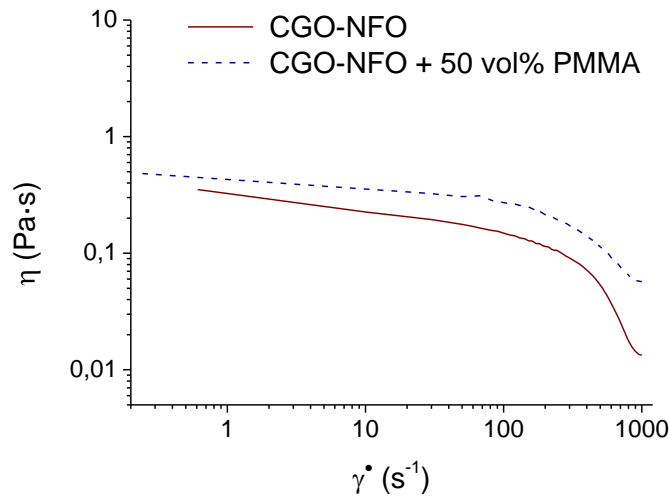
Figure 9 Logarithmic plot of the rheological behavior of the composite pastes

Both inks present a pseudoplastic behavior, i.e., viscosity decreases slightly with the shear rate until 400 s^{-1} and then it drops. This kind of behavior is appropriate for screen-printing technique because when the ink is squeezed, its viscosity is very low and can be deposited on the substrate and when the shearing is stopped, viscosity increases fast avoiding the spread on the surface.

In order to co-sinter both CGO-NFO layers and the 3YSZ substrate, the substrate was pre-treated at 1150ºC for 1 h, then top-layers were screen-printed and the complete assembly sintered at 1450ºC for 2 h. The microstructure of the deposited films was analyzed by SEM (*Figure 10*). *Figure 10*a shows the superficial microstructure at the edge of the deposited layers, where three areas can be observed: the substrate, the porous interlayer (CGO-NFO-PMMA) and the dense MIEC layer (CGO-NFO). The surface of the dense layer is shown in *Figure 10*b and the cross-section of the substrate and both layers in *Figure 10*c.
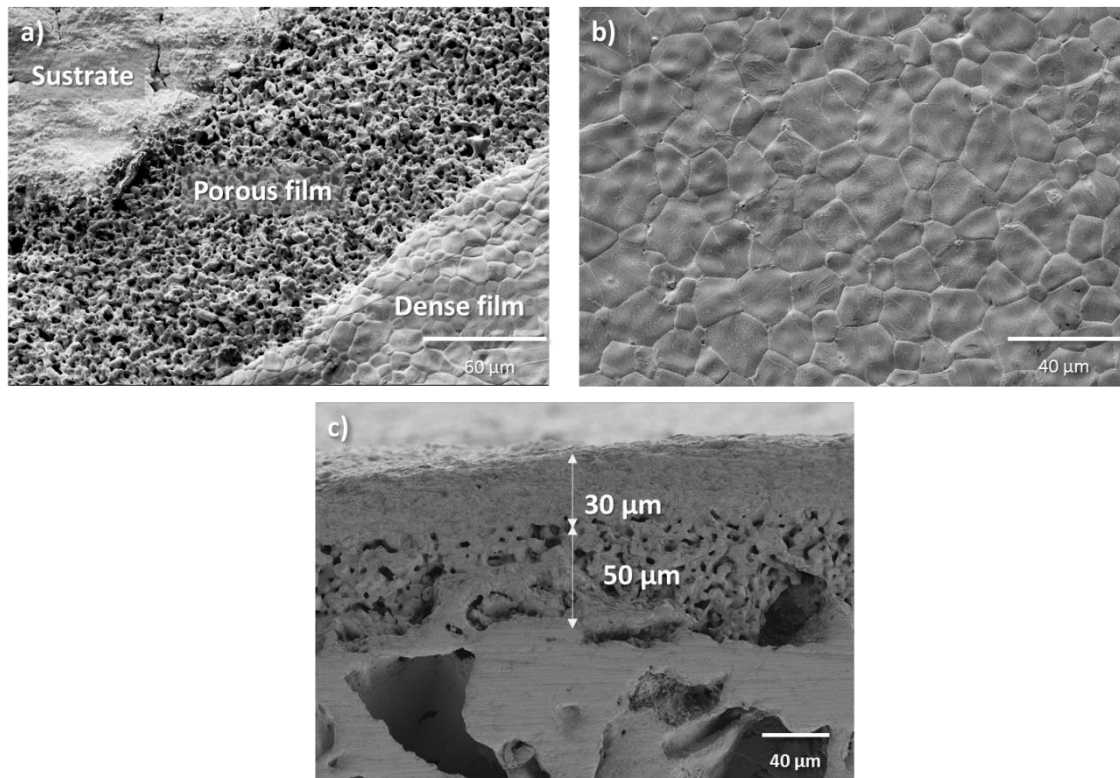
Figure 10 SEM images of the membranes: (a-b) top views and (c) polished cross-section

In order to characterize the membrane, the in-plane total conductivity of the top MIEC coatings was studied by 4-point DC measurements from 800 to 400 °C under different atmospheres (*Figure 11*a). *Figure 11*b shows the conductivity of the membrane as a function of the pO_2 at three different temperatures.
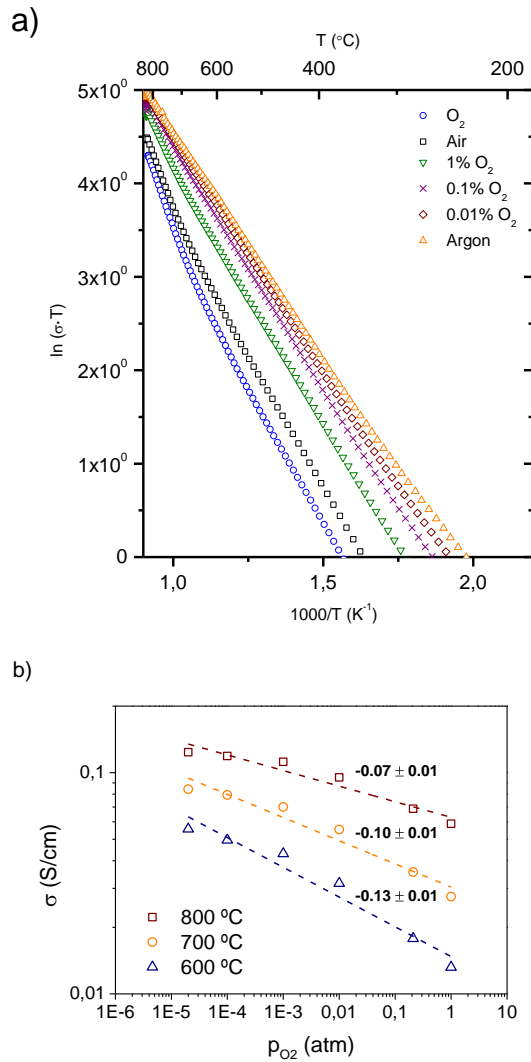
a)

b)

Figure 11 In-plane conductivity of a 30μm-thick CGO-NFO membrane at a) different atmospheres and b) at different temperatures as a function of O₂ partial pressure

3. Discussion

The zeta potential study allows preparing stable 3YSZ suspensions in water with 35 vol. % of solids for slip-casting. The rheological study presented in *Figure 4* compares the flow curves for 3YSZ suspensions with different amounts of pore former and their rheological parameters according to the Cross model (eq. 2). The incorporation of the S-050 particles to the slurries implies (1) the increase of the η_0 value and thus the sedimentation stability; and (2) the decrease in the viscosity at slip-casting shear rate ($100s^{-1}$) and the η_∞, which involves a less effective homogenization of the suspensions. Taking this into account, the addition of pore former enables to improve the slip-casting characteristics of the slurries.

The samples with 40 vol. % of pore former in the slurry composition are presented at the micrographs in *Figure 5*. The pores in these samples are spherical and the actual size and shape is directly related to the pore former particles added to the slurries. This porous system presents very low connectivity giving rise to a close porosity, which makes difficult the flow of the feed gas through the membranes. The Archimedes measurements for these samples (summarized in *Table 2*) revealed that a decrease in porosity of about 15% takes place during

the sintering process. The increment of the pore former volume fraction up to 60 vol. % in the slurry has a direct influence on the microstructure as shown in *Figure 6*. However, as for the case of the previous samples, the porosity obtained from spherical PMMA particles (*Figure 6*a and *Figure 6*b) presents low interconnectivity. On the other hand, the use of the flake-like PMMA particles seems to increase the contact between pores (*Figure 6*c) but is insufficient. The porosity values (*Table 2*) show a decrement of 12%-20% for the samples with spherical pore former particles, similar to the previous samples. The lowest loss in porosity is observed for the sample prepared with F-150 particles and the highest loss for the sample with the smallest pore former (S-006).

In order to improve the connectivity between pores, it was decided to use a combination of spherical (S-050) and flake-like particles in a 1:1 ratio, in a 60 vol. % (*Figure 7*). The resulting samples pieces present 50% of porosity with high interconnectivity, which improves the gas permeation through the substrate towards the MIEC layers. Therefore, this formulation was selected to prepare the substrates for the asymmetric membranes.

Suitability of the substrates was studied in terms of their resistance against an air flow, measuring their pressure drop. The obtained data, plotted at *Figure 8*, confirm that the use of a combination of F-150 and S-050 particles, in a total volume of 60% in the slurry composition, improves the permeation of the substrates.

As described before, the substrates where pre-treated at 1150ºC in air prior to CGO-NFO deposition, and later the complete assembly was sintered the membrane at 1450ºC. This procedure allows resembling the thermal expansion of the layers and substrate, and improving the final density of the dense layer due to the contraction of the substrate. *Figure 10*a shows a superficial view of both CGO-NFO layers and the substrate at the edge of the deposition, where the different in density and morphology between both screen-printed layers after sintering can be observed. The top layer of CGO-NFO presents a good sintering and high density as shown in the top view of the membrane (*Figure 10*b). These results are confirmed in the cross-section view of the membrane in *Figure 10*c, where the dense top layer 30 µm of thickness, and the interlayer 50 µm of thickness. It should be noted that the porosity of the interlayer is open with connectivity while the top-layer is gas tight.

The in-plane electrochemical measurements (*Figure 11*) show conductivity values above 50 $mS \cdot cm^{-2}$ and this conductivity level can only be related to electronic conduction. This evidences the presence of a percolating network of the NFO phase - electronic conducting phase of the composite. The conductivity values are in the same order of magnitude than that observed for NFO bulk (e.g. 250 $mS \cdot cm^{-2}$ at 800ºC in air) and thin-film samples [7] and this suggests that the electronic pathways are as abundant as ionic pathways. In principle, the conduction properties are acceptable for application as oxygen transport membrane. In general, the conductivity (*Figure 11*a) presents a simple Arrhenius behavior although the activation energy becomes slightly lower at temperatures below 600 ºC and this effect is more visible at high pO_2. *Figure 11*b reveals that the conductivity decreases with pO_2. This is another sign of the important contribution of electronic transport in the total transport in these deposited films. At 600ºC, the pO_2 dependence ($p''O_2$) follows a power law with exponent *n* close to -1/6, which is characteristic for n-type conductors. This result is in line with the n-type electronic character reported for monolith Tb-doped CeO_2-NFO composite membranes with different NFO contents [9,33]. The exponent value, *n*, becomes lower with increasing temperatures and this may be

ascribed to the higher contribution of ionic conduction and the reduction of electronic charge carrier concentration in the material (electrons) with increasing temperatures.

As a final test of the function of the membrane, the selective oxygen permeation was studied in the temperature range of 850-750 ºC under an Air/Argon gradient (300 ml·min^{-1} for both streams). *Figure 12* depicts the oxygen flux J(O$_2$) dependence with temperature for the membrane with support prepared with F-150 and S-050 pore formers . An oxygen flux of ca. 0.5 ml·min^{-1}·cm^{-2} is obtained at 850 ºC, whereas at 750 ºC J(O$_2$) decreases to 0.075 ml·min^{-1}· cm^{-2}. Moreover, the oxygen permeation results of a 0.8 mm-thick membrane are presented with the aim of studying the effect of thickness reduction. Despite the membranes were tested in different temperature ranges, a fair comparison can be performed by interpolating available J(O$_2$) values at higher temperatures, taking into account that these membranes typically present a change in the Ea above 800 ºC [33–35]. Therefore, a significant improvement in oxygen permeation can be observed for the thinner membrane, with a 1.000-fold improvement at 850 ºC and an expected 40-times gain in J(O$_2$) at 950 ºC. Due to the interpolation, this improvement may be handled as an approximation. Nevertheless, the improvement in the permeation flux thanks to thickness reduction achieved in the supported membrane is very visible.
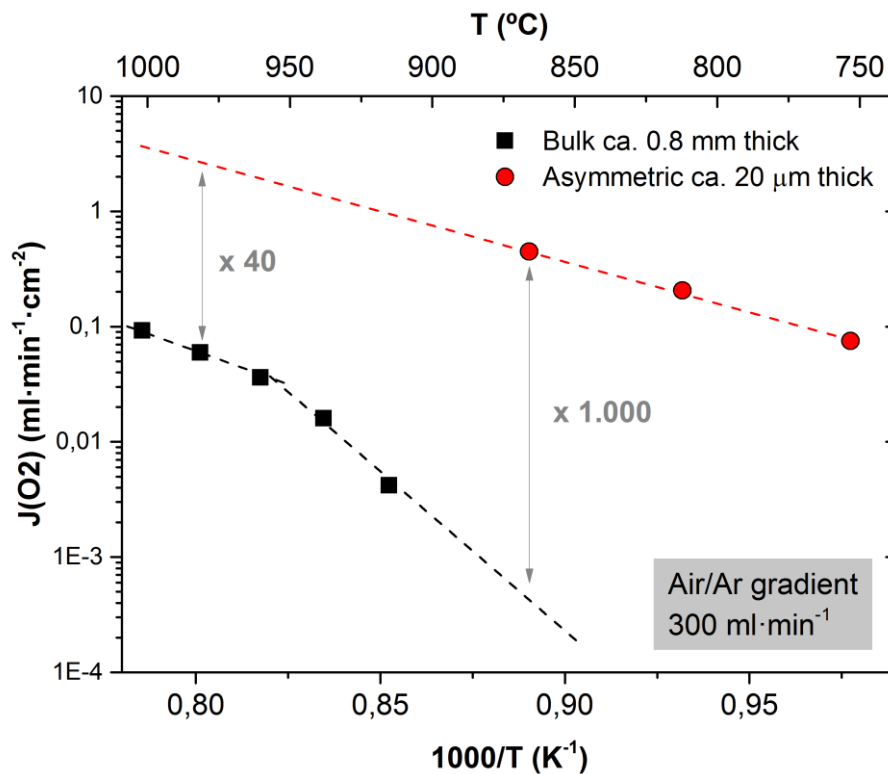
Figure 12 Comparison of the oxygen fluxes as a function of the temperature between a bulk membrane of CGO-NFO and the asymmetric membrane presented in this paper

4 Conclusions

The main conclusions and achievements of the present study on the manufacture by slip-casting and characterization of 3YSZ supports for O_2-separation membranes are:

- Stable aqueous suspensions of YSZ and PMMA particles were formulated. PMMA is employed as pore former and different particle sizes and morphologies were considered.

- The effect of the PMMA volume in the slip as well as its particle size and morphology were studied. Namely, the effect on the porosity magnitude and nature, and the permeation resistance was characterized. In this sense, the combination of spherical and flake-like PMMA particles in a 60 vol. % in the slip make it possible to produce open porosity in the YSZ substrates suitable for fast gas diffusion.

- Complete O_2-separation membranes were prepared by depositing by screen-printing two top layers made of CGO-NFO, a mixed ionic-electronic composite material: (1) a porous interlayer –acting as gas diffusion layer and catalytic layer; and (2) a dense and 20-30μm gastight film, for the selective oxygen separation.

- CGO-NFO asymmetric membranes with 3YSZ substrate obtained by slip casting showed promising O_2 production features, with better results than a monolithic CGO-NFO membrane in preliminary studies.

- Slip casting processing route opens the door to obtain MIEC membranes with complex shapes that can meet the necessary requirements depending on their application either as O_2 separators or catalytic membrane reactors for oxidative conversions.

5. Acknowledgements

6 References

[1]   S.S. Hashim, A.R. Mohamed, S. Bhatia, Oxygen separation from air using ceramic-based membrane technology for sustainable fuel production and power generation, Renew. Sustain. Energy Rev. 15 (2011) 1284–1293. doi:10.1016/j.rser.2010.10.002.

[2]   T. Takahashi, T. Esaka, H. Iwahara, Electrical conduction in the sintered oxides of the system Bi2O3BaO, J. Solid State Chem. 16 (1976) 317–323. doi:10.1016/0022-4596(76)90047-5.

[3]   B. Cales, J.F. Baumard, Oxygen semipermeability and electronic conductivity in calcia-stabilized zirconia, J. Mater. Sci. 17 (1982) 3243–3248. doi:10.1007/BF01203490.

[4]   J. Sunarso, S. Baumann, J.M. Serra, W.A. Meulenberg, S. Liu, Y.S. Lin, et al., Mixed ionic–electronic conducting (MIEC) ceramic-based membranes for oxygen separation, J. Memb. Sci. 320 (2008) 13–41. doi:10.1016/j.memsci.2008.03.074.

[5]   J.H. Joo, K.S. Yun, J.H. Kim, Y. Lee, C.Y. Yoo, J.H. Yu, Substantial Oxygen Flux in Dual-Phase Membrane of Ceria and Pure Electronic Conductor by Tailoring the Surface, ACS

Appl. Mater. Interfaces. 7 (2015) 14699–14707. doi:10.1021/acsami.5b03392.

[6]   W. Fang, F. Liang, Z. Cao, F. Steinbach, A. Feldhoff, A mixed ionic and electronic conducting dual-phase membrane with high oxygen permeability, Angew. Chemie - Int. Ed. 54 (2015) 4847–4850. doi:10.1002/anie.201411963.

[7]   C. Solis, S. Somacescu, E. Palafox, J.M. Serra, Particular Transport Properties of NiFe2O4 Thin Films at High Temperatures, (2014) 2–4.

[8]   C. Gaudillère, L. Olivier, P. Vernoux, C. Zhang, Z. Shao, D. Farrusseng, Alternative perovskite materials as a cathode component for intermediate temperature single-chamber solid oxide fuel cell, J. Power Sources. 195 (2010) 4758–4764. doi:10.1016/j.jpowsour.2010.02.058.

[9]   M.P. Lobera, J.M. Serra, S.P. Foghmoes, M. Søgaard, A. Kaiser, On the use of supported ceria membranes for oxyfuel process/syngas production, J. Memb. Sci. 385-386 (2011) 154–161. doi:10.1016/j.memsci.2011.09.031.

[10]   V. V. Zyryanov, V.A. Sadykov, G.M. Alikina, Design of Multilayer Ceramic MIEC Membranes, Sep. Sci. Technol. 42 (2007) 2849–2861. doi:10.1080/01496390701558300.

[11]   P. Pandey, R.S. Chauhan, Membranes for gas separation, Prog. Polym. Sci. 26 (2001) 853–893. doi:10.1016/S0079-6700(01)00009-0.

[12]   S. Baumann, W.A. Meulenberg, H.P. Buchkremer, Manufacturing strategies for asymmetric ceramic membranes for efficient separation of oxygen from air, J. Eur. Ceram. Soc. 33 (2013) 1251–1261. doi:10.1016/j.jeurceramsoc.2012.12.005.

[13]   Y. Gu, G. Meng, A model for ceramic membrane formation by dip-coating, J. Eur. Ceram. Soc. 19 (1999) 1961–1966. doi:10.1016/S0955-2219(99)00013-8.

[14]   J.M. Serra, J. Garcia-Fayos, S. Baumann, F. Schulze-Küppers, W.A. Meulenberg, Oxygen permeation through tape-cast asymmetric all-La0.6Sr0.4Co0.2Fe0.8O3−δ membranes, J. Memb. Sci. 447 (2013) 297–305. doi:10.1016/j.memsci.2013.07.030.

[15]   P. Pinacci, E. Louradour, L. Wimbert, M. Gindrat, M.O. Jarligo, R. Vassen, et al., Dense membranes for oxygen and hydrogen separation (DEMOYS): project overview and first results, Energy Procedia. 37 (2013) 1030–1038. doi:10.1016/j.egypro.2013.05.199.

[16]   P. Lemes-rachadel, G. Sachinelli, R. Antonio, F. Machado, Current Developments of Mixed Conducting Membranes on Porous Substrates, 17 (2014) 242–249.

[17]   S. Pirou, J. Gurauskis, V. Gil, M. Sogaard, P.V. Hendriksen, A. Kaiser, et al., Oxygen permeation flux through 10Sc1YSZ-MnCo2O4 asymmetric membranes prepared by two-step sintering, Fuel Process. Technol. 152 (2016) 192–199. doi:10.1016/j.fuproc.2016.06.019.

[18]   E. Mercadelli, D. Montaleone, A. Gondolini, P. Pinasco, A. Sanson, Tape-cast asymmetric membranes for hydrogen separation, Ceram. Int. (2017). doi:10.1016/j.ceramint.2017.03.099.

[19]   C. Gaudillere, J.M. Serra, Freeze-casting: Fabrication of highlyporous and hierarchical ceramic supports for energy applications, Bol. La Soc. Esp. Ceram. Y Vidr. 55 (2016) 45–54. doi:10.1016/j.bsecv.2016.02.002.

[20]   J. Seuba, J. Leloup, S. Richaud, S. Deville, C. Guizard, A.J. Stevenson, Fabrication of ice-templated tubes by rotational freezing: microstructure, strength, and permeability, J.

Eur. Ceram. Soc. 37 (2016) 2423–2429. doi:10.1016/j.jeurceramsoc.2017.01.014.

[21] A. V. Kovalevsky, V. V. Kharton, F.M.M. Snijkers, J.F.C. Cooymans, J.J. Luyten, J.R. Frade, Processing and oxygen permeability of asymmetric ferrite-based ceramic membranes, Solid State Ionics. 179 (2008) 61–65. doi:10.1016/j.ssi.2007.12.027.

[22] A.V. Kovalevsky, A.A. Yaremchenko, V.A. Kolotygin, F.M.M. Snijkers, V.V. Kharton, A. Buekenhoudt, et al., Oxygen permeability and stability of asymmetric multilayer Ba0.5Sr0.5Co0.8Fe0.2O3−δ ceramic membranes, Solid State Ionics. 192 (2011) 677–681. doi:10.1016/j.ssi.2010.05.030.

[23] S. Ovtar, J. Gurauskis, A. Bj??rnetun Haugen, C. Chatzichristodoulou, A. Kaiser, P.V. Hendriksen, Oxygen transport properties of tubular Ce0.9Gd0.1O1.95-La0.6Sr0.4FeO3???d composite asymmetric oxygen permeation membranes supported on magnesium oxide, J. Memb. Sci. 523 (2017) 576–587. doi:10.1016/j.memsci.2016.09.060.

[24] Z. Liu, G. Zhang, X. Dong, W. Jiang, W. Jin, N. Xu, Fabrication of asymmetric tubular mixed-conducting dense membranes by a combined spin-spraying and co-sintering process, J. Memb. Sci. 415-416 (2012) 313–319. doi:10.1016/j.memsci.2012.05.011.

[25] M.B. Choi, D.K. Lim, S.Y. Jeon, H.S. Kim, S.J. Song, Oxygen permeation properties of BSCF5582 tubular membrane fabricated by the slip casting method, Ceram. Int. 38 (2012) 1867–1872. doi:10.1016/j.ceramint.2011.10.012.

[26] J.A. Queiroga, E.H.M. Nunes, D.F. Souza, D.C.L. Vasconcelos, V.S.T. Ciminelli, W.L. Vasconcelos, Microstructural investigation and performance evaluation of slip-cast alumina supports, (2016). doi:10.1016/j.ceramint.2016.12.037.

[27] C. Ceramics, Porous Ceramic Processing, (n.d.) 1–4.

[28] P. Monash, G. Pugazhenthi, P. Saravanan, Various fabrication methods of porous ceramic supports for membrane applications, Rev. Chem. Eng. 29 (2013) 357–383. doi:10.1515/revce-2013-0006.

[29] J.A. Lewis, Colloidal Processing of Ceramics, 59 (2000) 2341–2359.

[30] A.R. Studart, E. Amstad, L.J. Gauckler, Colloidal stabilization of nanoparticles in concentrated suspensions., Langmuir. 23 (2007) 1081–90. doi:10.1021/la062042s.

[31] L.J. Gauckler, T. Graule, F. Baader, Ceramic forming using enzyme catalyzed reactions, Mater. Chem. Phys. 61 (1999) 78–102. doi:10.1016/S0254-0584(99)00117-0.

[32] W. Loop, Water Absorption, Bulk Density, Apparent Porosity, and Apparent Speci c Gravity of Fired Whiteware Products 1, 88 (2009) 13–14. doi:10.1520/C0373-88R06.edges.

[33] J. Garcia-Fayos, M. Balaguer, J.M. Serra, Dual-Phase Oxygen Transport Membranes for Stable Operation in Environments Containing Carbon Dioxide and Sulfur Dioxide, ChemSusChem. 8 (2015) 4242–4249. doi:10.1002/cssc.201500951.

[34] M. Balaguer, J. García-Fayos, C. Solís, J.M. Serra, Fast Oxygen Separation Through SO2 - and CO2 -Stable Dual-Phase Membrane Based on NiFe 2 O 4 –Ce 0.8 Tb 0.2 O 2-δ, Chem. Mater. 25 (2013) 4986–4993. doi:10.1021/cm4034963.

[35] C. Gaudillere, J. Garcia-Fayos, J.M. Serra, Enhancing oxygen permeation through hierarchically-structured perovskite membranes elaborated by freeze-casting, J. Mater. Chem. A. 2 (2014) 3828. doi:10.1039/c3ta14069e.